Hindawi
Journal of Nanomaterials
Volume 2018, Article ID 9326408, 8 pages
https://doi.org/10.1155/2018/9326408

Research Article

Self-Ordered Voids Formation in SiO_2 Matrix by Ge Outdiffusion

B. Pivac,[1] **P. Dubček**,[1] **J. Dasović**,[1] **H. Zorc**,[1] **S. Bernstorff**,[2] **J. Zavašnik**,[3] **and B. Vlahovic**[4]

[1] *Ruđer Bošković Institute, Bijenička 54, 10000 Zagreb, Croatia*
[2] *Elettra-Sincrotrone Trieste, SS 14, Km 163.5, 34149 Basovizza, Italy*
[3] *Center for Electron Microscopy and Microanalysis, Jožef Stefan Institute, Jamova Cesta 39, SI-1000 Ljubljana, Slovenia*
[4] *North Carolina Central University, Durham, NC, USA*

Correspondence should be addressed to B. Pivac; pivac@irb.hr

Received 7 December 2017; Accepted 12 March 2018; Published 26 April 2018

Academic Editor: Iftikhar Ali Sahito

The annealing behavior of very thin SiO_2/Ge multilayers deposited on Si substrate by e-gun deposition in high vacuum was explored. It is shown that, after annealing at moderate temperatures (800°C) in inert atmosphere, Ge is completely outdiffused from the SiO_2 matrix leaving small (about 3 nm) spherical voids embedded in the SiO_2 matrix. These voids are very well correlated and formed at distances governed by the preexisting multilayer structure (in vertical direction) and self-organization (in horizontal direction). The formed films produce intensive photoluminescence (PL) with a peak at 500 nm. The explored dynamics of the PL decay show the existence of a very rapid process similar to the one found at Ge/SiO_2 defected interface layers.

1. Introduction

An enhancement of the absorption in the visible range is crucial for increasing the conversion efficiency of solar cells. Recently, several attempts have been made to use photonic crystals for enhancing light absorption in thin layers [1–3]. But the specific design of possible new photovoltaic devices is still an open discussion, and definite guidelines for reliable light absorption enhancement have not been proposed.

Silicon dioxide, which is transparent at visible wavelengths, is fully compatible with Si technology, and due to its low cost it is interesting as a potential photonic material. Indeed a successful application of silica in photonics has been demonstrated [4, 5]. Furthermore, it has been recently shown that the use of silica based photonic crystals significantly contributes to radiative cooling of solar absorbers and hence increases their efficiency of solar energy conversion [6]. Among other applications, the fabrication of void arrays in the bulk of dielectrics has drawn great attention for its potential applications in three-dimensional (3D) optical storage, photonic crystal, and integrated optics [7]. Since the early observation of femtosecond-laser induced periodically aligned nanovoids inside conventional borosilicate glass by Kanehira et al. in 2005 [8], many groups have been devoted to exploring the applications and formation mechanisms of self-organized void arrays.

Many other different ways to produce porous SiO_2 layers have been explored. Recently it has been shown that Ge implantation in fused silica followed by annealing creates spherical voids in the matrix with dimensions of few to few tenths of nanometers [9, 10]. In the following a new and rather simple procedure for transparent silica photonic layer production will be proposed, based on Ge outdiffusion and void formation and self-organization in silica matrix.

2. Experimental

2.1. Sample Preparation. A multilayer film consisting of alternating SiO_2 and Ge layers, each 2 nm thick, was prepared by e-gun deposition of 20 bilayers, in vacuum better than 10^{-6} Torr. The solid sources for the SiO_2 and Ge layer deposition were grains (4 N and 6 N purity, resp., from

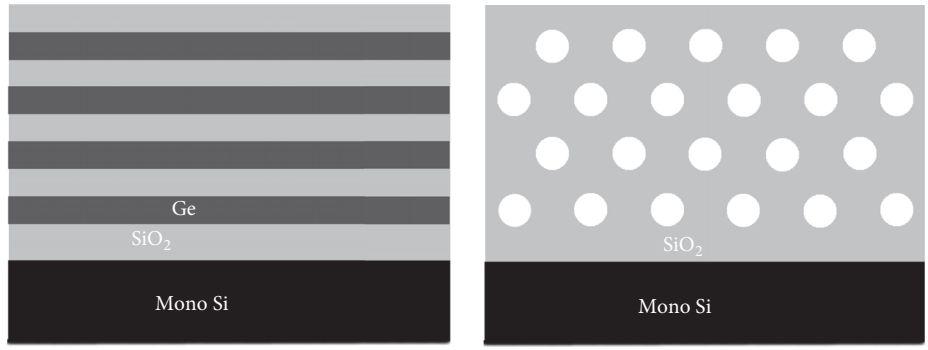

Figure 1: Schematic representation of an as-deposited 2 nm SiO_2/2 nm Ge multilayer with a 20 nm SiO_2 capping layer at the top (a) and after annealing at 800°C, showing cavities (white) in SiO_2 matrix (b).

Alfa Res.). Cleaned and freshly etched p-type (100)-oriented Si monocrystals were used as substrates, held at 200°C during the deposition. The Si substrates were rotated on a planetary holder during the deposition to ensure lateral homogeneity of the films over the whole substrate surface. After deposition, the samples were annealed at 800°C for 1 h in flowing N_2 atmosphere. During this annealing Ge initially clusters into nanoparticles [11] and afterwards outdiffuses from the film (below the measurable level of Raman and XRD spectroscopy). Finally layers of cavities were obtained separated by the approx. 2 nm of SiO_2 spacer layer is shown schematically in Figure 1.

2.2. Characterization Procedure. Grazing incidence small-angle X-ray scattering (GISAXS) experiments were performed at Elettra-Sincrotrone, Trieste, Italy, on the SAXS beamline [12], using synchrotron radiation with photon energy of 8 keV. Several grazing angles of incidence α_i were selected in the range $0.23^\circ < \alpha_i < 0.23^\circ + 0.1^\circ$, for which the effective area of the beam footprint was smaller than the sample surface area (approx. 10×10 mm). The selected angles above the critical angle α_c allowed the X-rays to penetrate through the capping layer and deep enough into the film. The angular range of the detector was calibrated by measuring the SAXS standard silver behenate. A narrow, partly transparent Al strip was placed in front of the detector for local intensity reduction in order to avoid saturation in the specular plane direction where the usually much stronger surface scattering is present.

Two-dimensional patterns of the scattering intensity were recorded with a 2D image plate detector with 2000×2000 pixels, having a dynamical range of 10^6 and a pixel size of 0.2×0.2 mm, at the distance $L = 1800$ mm from the sample. The optical path from the sample to the detector was kept in vacuum in order to reduce the background due to air scattering.

Raman spectra were acquired on a Labram HR Evolution system equipped with a microscope and a 473 nm laser excitation source.

The optical reflectivity in the UV-Vis range was measured with a Perkin Elmer Lambda 45 spectrometer with a gold mirror as reference.

Photoluminescence (PL) was measured at room temperature using a continuous wave laser diode at 405 nm, and the PL spectra were collected using a BWTek BCR 112E spectrometer coupled with a Sony ILX511 CCD linear image sensor.

The crystallinity and phase composition of the nanoparticles were analysed with an aberration-corrected transmission electron microscope (TEM), operating at 300 keV and capable of chemical analyses by employing energy dispersive X-ray spectroscopy (EDS). Samples for the TEM study were prepared as cross-sections of thin films. These were glued face-to-face with an epoxy resin, formatted into 3 mm disks and mechanically thinned to approximately 100 μm. The central part of the disks was additionally dimpled on a rotation wheel down to 10 μm and ion-milled with Ar+ ions at 4 keV until perforation.

3. Results and Discussion

The results of the Raman spectroscopy, shown in Figure 2, confirm the existence of Ge layers alternated with SiO_2 layers in the as-deposited sample. This sample, represented by the black curve, shows the presence of amorphous Ge layers with characteristic broad peaks close to 90, 190, 240, and 279 cm^{-1} corresponding to the Ge TA, LA, and LO modes, respectively [13]. The peak at 520 cm^{-1} is due to the Si TO mode derived from the substrate. After annealing at 800°C or higher Ge was not anymore observed in the sample (within the sensitivity of the employed Raman instrument). The only peak observed for the annealed sample, at 521 cm^{-1}, is due to the TO band from the silicon substrate. The same behavior was verified with X-ray diffraction (not shown here).

Since Ge was not anymore observable (by Raman and XRD spectroscopy) upon annealing at high temperatures, in order to explore the remaining structures in the sample, several techniques were considered. Scanning electron microscopy has the intrinsic difficulty of surface charging

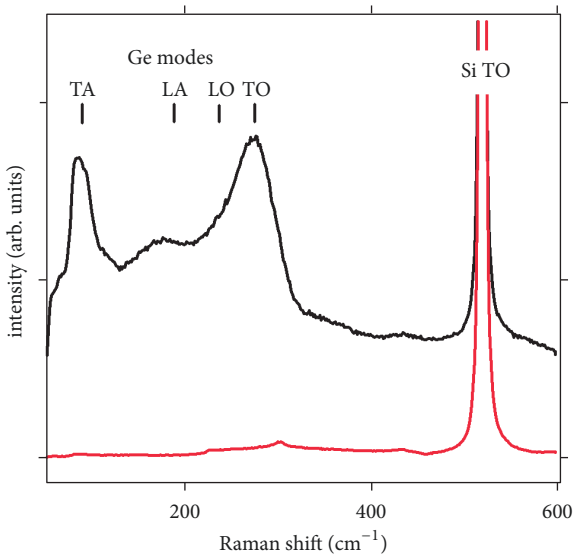

FIGURE 2: Raman spectra of an as-deposited (black), and an annealed at 800°C (red) multilayer sample.

in dielectrics which is usually removed by covering the sample surface with an Au layer. Since we expected to explore structures (voids) with sizes of less than 5 nm a metal cover could mask the structures of interest, which indeed happened in several our attempts. Therefore as measuring technique of choice for such a task grazing incidence small-angle X-ray scattering (GISAXS) was selected.

It is long known that with X-ray scattering complementary information (to microscopy results) can be obtained in reciprocal space. However, for a long time, the weak interaction of hard X-rays with matter hampered its straightforward use for surface and/or interface studies. Nevertheless, pioneering works in the 80s [14], combining the use of high brilliance synchrotron radiation with grazing incidence geometry, enabled reaching sufficient surface sensitivity with a reasonable signal to noise ratio. In comparison to conventional microscopy, GISAXS [15] has several advantages:

(i) It is a nondestructive technique, provided that the samples withstand hard X-ray exposure.

(ii) each measurement is averaging over the whole measured sample surface, providing therefore statistical information over several square centimeters as compared to nanoregions in microscopy;

(iii) Depth profiling of the samples can be easily performed by varying the grazing incident angle of the X-rays beam, which allows probing selectively the surface, buried interfaces, and the bulk of a sample;

(iv) The GISAXS technique provides morphological information from the nanometer to micrometer length scales. Furthermore, it can be combined, simultaneously and on the same samples, with the grazing incidence wide angle X-ray scattering or diffraction (GIWAXS) technique which is sensitive to the atomic arrangement and strain state.

2D GISAXS patterns obtained from the sample annealed at 800°C are presented in Figure 3. Here (in Figure 3(a)) the X-ray scattering originating from nanoparticles or voids embedded in the bulk is mixed with the one caused by the surface morphology and the roughness of the interface between layers, which are dominantly contributing to the signal close to the specular plain. Therefore the scattering, there, is generally most intense (this is the reason why a narrow Al foil was placed in the beam path, to partly attenuate the strong intensity signal in the specular plain).

The specific shape with two shoulders close to the Yoneda plain (q_z close to 0.2 nm^{-1}) visible in Figure 3(b) suggests X-ray scattering from correlated objects in the sample. Nevertheless, a scattering contribution from the very surface cannot be excluded. To remove the contribution from the roughness originating dominantly from the surface, the intensity taken at the critical angle in Figure 3(a) was subtracted numerically from the intensity obtained at a larger angle of grazing incidence (i.e., 0.038° above the critical angle) shown in Figure 3(b), displaying therefore only the contribution derived from the deeper regions of the film (Figure 3(c)) [16]. The differential result obtained in this way confirms that the observed nanoparticles exist deeper inside the films.

In the first approximation, it was assumed that the spherical voids are grown evenly distributed throughout the film. For such case a scattering model was developed, where the particles radius R is allowed to vary according to a normal size distribution. The spatial distribution of the particles is described by the local monodisperse approximation (LMA). Applying numerical fitting to the measured experimental data of Figure 3(b), a wide size distribution for the voids diameter (D) was found, centered at $D_h = 2.95 \pm 0.35$ nm in horizontal direction and $D_v = 2.33 \pm 0.31$ nm in vertical direction. Thus the fitting revealed that the voids are spherical with only a very small eccentricity.

In Figure 4 the fitting results for the scattering pattern of Figure 3(b) are summarized and presented as voids size distribution in vertical and horizontal directions. When the fitting was applied to the scattering data after subtracting the surface scattering (Figure 3(c)), the distributions of the size values get wider and slightly shifted in direction of bigger particles as compared to the fitting results obtained for Figure 3(b). This is explained by the influence of surface features which are generally smaller than the voids formed inside the film.

Due to the precise deposition of well-defined multilayered SiO_2/Ge layers, after annealing well-defined layers of cavities were obtained at the positions where the Ge layers used to be prior to annealing. This causes the appearance of a Bragg sheet [17] in Figures 3(a) and 3(b) at about $q_z = 1.3$ nm^{-1} parallel to the q_y axis due to the periodicity contrast of the void layers. The period d of the void layers is calculated from the Bragg sheet position by the expression $d = 2\pi/q_z$, where q_z is the distance to the maximum of the first Bragg sheet. The measured period is $d = 4.8$ nm, very close to the original bilayer thickness.

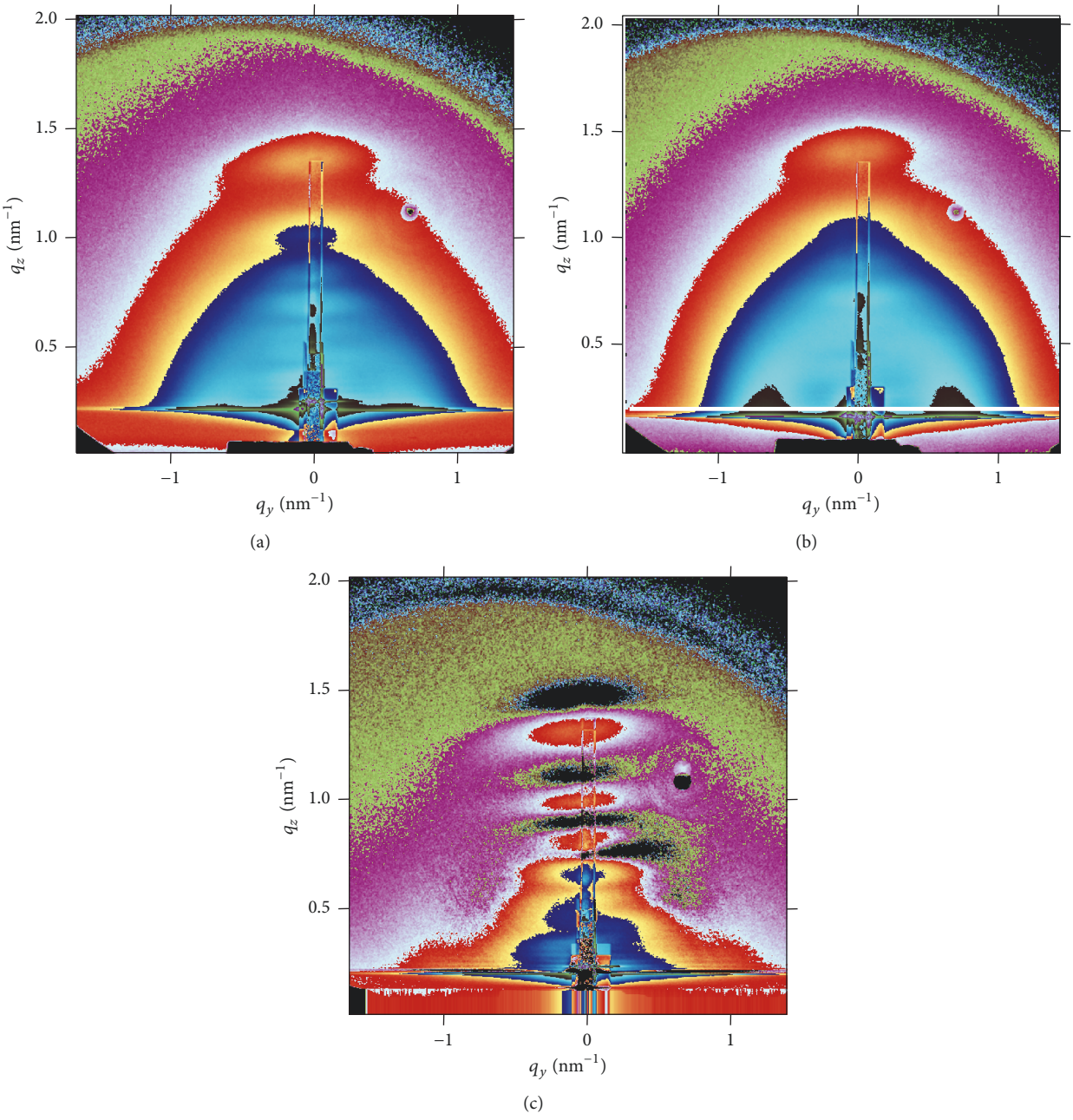

FIGURE 3: 2D GISAXS intensity pattern from the sample annealed at 800°C obtained (a) at the critical angle of grazing incidence α_c. The white line represents the Yoneda plain position where the linear intensity plot for the correlation analysis was taken. (b) 2D GISAXS pattern from the sample obtained at $\alpha_c + 0.038°$. (c) Numerical difference between the intensities from (b) and (a) (see the text for details).

A horizontal cut taken from the 2D scattering pattern shown in Figure 3(b) at the position of the horizontal white line is presented in Figure 5. The figure shows two very pronounced correlation peaks placed at about $q_y = \pm 1.3\,\text{nm}^{-1}$, indicating a rather strong correlation of the average voids interspacing in horizontal direction. Therefore, it was shown that in addition to the vertical ordering defined by the multilayer deposition, horizontal self-ordering has been obtained also. Furthermore, from the fitting procedure the void-to-void distance in horizontal direction is obtained as 7.03 ± 1.85 nm and in vertical direction as 4.29 ± 1.84 nm. The results for the diameters and distance between the voids in horizontal and vertical directions are summarized in Figure 4.

Looking carefully at the intensity distribution, one can see that the correlation is present in all the directions as shown in Figure 6. The figure is constructed of consecutive q_y = const. cut plots for the range above the Yoneda plain. The correlation peak forms a ring around the direct beam as indicated in Figure 6 with a transparent blue line. Since the

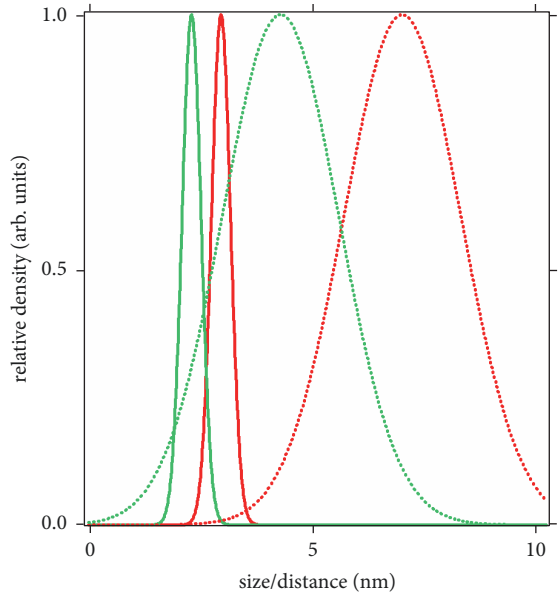

Figure 4: Distribution of void diameters (full lines) and correlation distances (dotted lines) for vertical (green lines) and horizontal (red lines) direction.

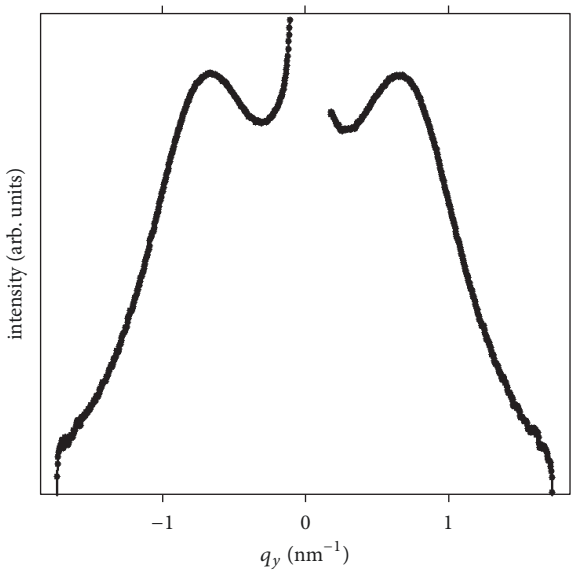

Figure 5: GISAXS intensity parallel to the sample surface taken at $q_z = 0.2\,\text{nm}^{-1}$ (see two-dimensional GISAXS pattern in Figure 3(b)) for the annealed film.

voids are concentrated within the previously Ge containing layer, the correlation peak is strongest at the Yoneda plain, where scattering is parallel to this plain. In the perpendicular direction the correlation is enhanced into the Bragg peak as the periodicity of void layer positions is preserved after annealing. The slight variation in the voids position in vertical direction within the layers results in a correlation peak spreading from the Yoneda plain up, with the intensity rapidly decreasing due to the lower concentration of the offset voids. Namely, the deposited layers are not perfectly flat, but some

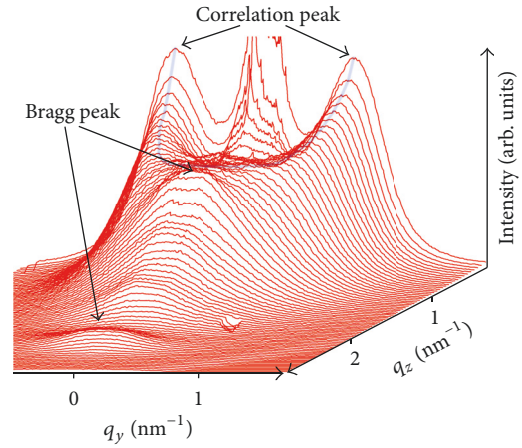

Figure 6: 3D plot of GISAXS intensities for the annealed sample. The Bragg sheets are indicated, as well as the signal maxima, due to the correlation (the transparent blue line).

surface roughness is present in the underlying layers and this is propagated upwards, with the upper layers thickness remaining more or less constant.

To support our findings we performed cross-section TEM analysis of the annealed samples where voids have been detected by GISAXS. Indeed as shown in Figure 7 the presence of voids is clearly evidenced. Each void measures approximately 5 nm in diameter. STEM-EDS mapping of the Si, Ge, and O distribution was performed on the same sample (selected area ROI, shown in Figure 7(a)). Although undetectable by Raman and XRD, Ge is still present in the layer and is homogeneously distributed throughout the layer (however, small Ge-free areas show the presence of voids).

Figure 8 shows the UV-VIS reflectance of the as-deposited SiO_2/Ge multilayer superstructure which could be used as antireflectance coating, since the reflectance is strongly reduced with respect to the Si substrate in the whole measured range. Quite similar is the behavior of the pure SiO_2 layer deposited on Si, in the spectral range $\lambda > 500$ nm. During annealing at 800°C the investigated sample substantially became a SiO_2 layer with voids and a small remaining part of Ge (as revealed by EDS microscopy) and shows qualitatively a similar behavior as an amorphous SiO_2 layer. The reflectance of a clean Si substrate is also added to Figure 8 as a reference.

Silicon rich layers [18] and/or SiO_2/Ge multilayers [19], after annealing at appropriate temperatures, produce a significant PL signal which indicates that structural changes, that is, nanoparticles or voids, developed in the films. In order to check the effect of voids creation within a SiO_2 matrix the PL was measured from SiO_2 layers with voids and compared with the PL from as-deposited SiO_2/Ge multilayers; see Figure 9. A very intensive PL peak centered at about 500 nm can be seen. Such signal, but with lower intensity, was already observed in samples with Ge nanoparticles and attributed to defective SiO_x nanolayers close to the Ge/SiO_2 interface [19].

The emission and relaxation dynamics of this peak was explored and the results are given in the inset of Figure 9. The

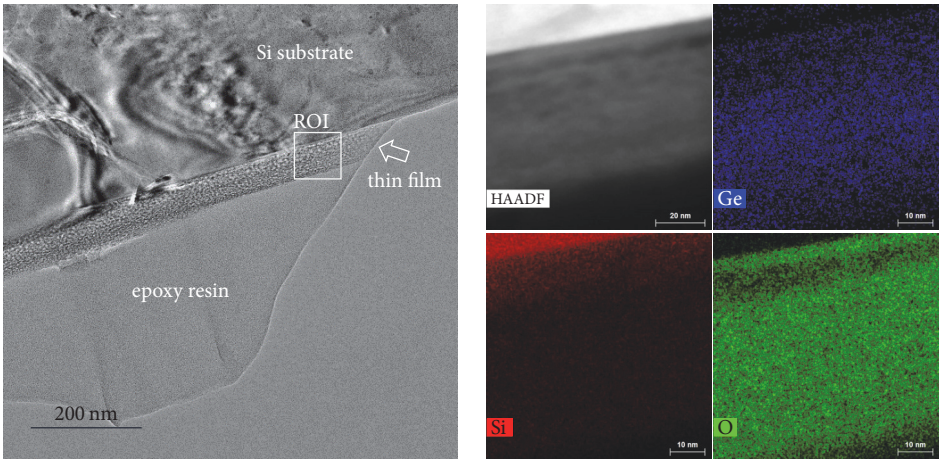

Figure 7: (a) Overview bright-field TEM micrograph of an annealed sample, showing the single-crystal Si substrate at the top, followed by layered voids formed in the amorphous SiO_2 thin-film layer. The thickness of the whole thin-film layer at this point is 60 nm. The rectangular region of interest (ROI) was analysed in detail in (b), where STEM-EDS mappings of the fine structures were performed.

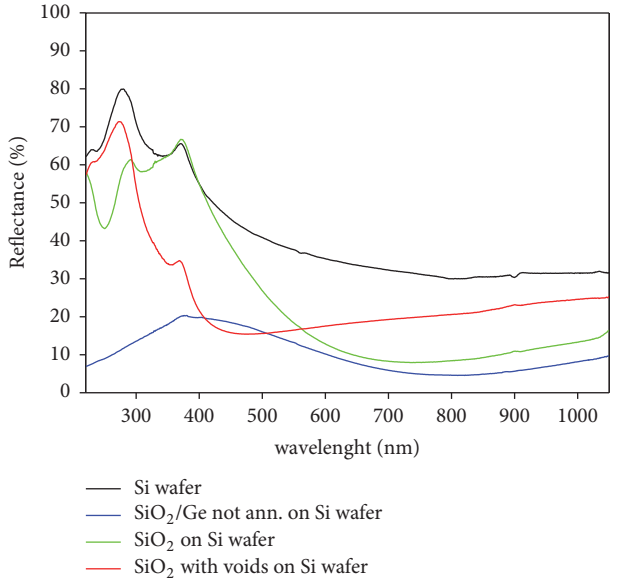

Figure 8: UV-Vis reflectance spectra of the as-deposited sample (SiO_2/Ge multilayers, blue curve), annealed sample (substantially SiO_2 with voids, red curve), and pure silica layer of the same thickness (green curve) on Si substrate. The clean Si substrate was also measured for comparison (black curve).

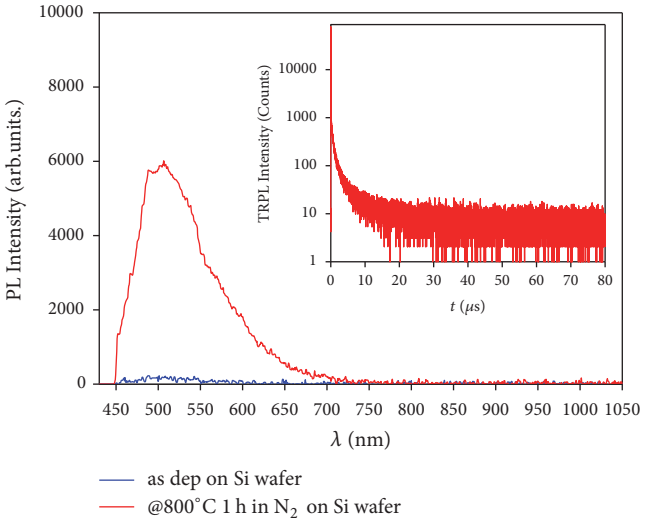

Figure 9: PL spectra of as-deposited (blue) and annealed (red, with voids) silica layer on Si substrate. The inset shows the time-resolved photoluminescence obtained from the annealed sample, recorded at 375 nm excitation wave length.

decay curve has been fitted using two stretched exponential functions according to the expression:

$$I(t) = I_0 \exp - \left(\frac{t}{\tau_{1,2}} \right) \beta_{1,2}, \quad (1)$$

where $\tau_{1,2}$ are the PL lifetimes and $0 \leq \beta_{1,2} \leq 1$ are the dispersion exponents. The corresponding PL lifetimes and stretching constants are $t_1 = 139 \pm 15$ ns with $\beta_1 = 0.33 \pm 0.01$ and $t_2 = 7.0 \pm 0.7$ ns with $\beta_2 = 0.30 \pm 0.01$. These results are similar to previous findings in samples with Ge nanodots in silica matrix [13], where it was concluded that the PL is due to defected SiO_x layers at the interface between Ge nanodots and the silica matrix. Likewise, here the PL originates from the border region around the voids.

To further confirm our statement that voids formed in SiO_2 matrix after a major Ge outdiffusion from the multilayer sample, the GISAXS results were analysed in the light of the Porod theory [20] and are presented in Figure 10. Assuming that the thickness of the shell enveloping the voids has a uniform thickness D, it is possible to estimate the parameter

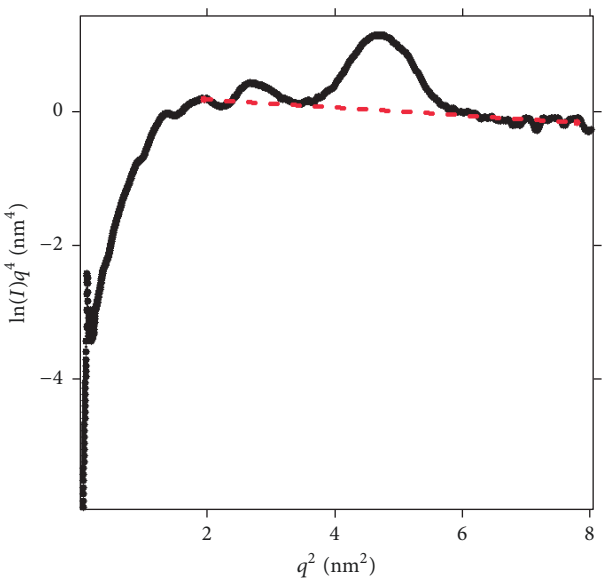

FIGURE 10: Plot of GISAXS intensity in the form $\ln[q^4 I(q)]$ versus q^2 for the SiO_2/Ge 2/2 nm sample, annealed at 800°C and thus containing voids embedded in the SiO_2 matrix. For $q^2 > 6\,\text{nm}^{-2}$ the straight line (to the detector limit for the applied setup) shows the fit from which the thickness of the border region around the voids is calculated. The peak at $q^2 = 4.5\,\text{nm}^{-2}$ represents the Bragg peak.

σ of the layer, which describes the electron density gradient through [21]

$$\ln\left[q^4 I\left(q\right)\right] = \ln K - \sigma^2 q^2, \tag{2}$$

where q is the wave vector, I is the GISAXS intensity, and K is a constant.

The layer thickness D is related to σ by $D = (2\pi)^{1/2}\sigma$ and was calculated to be 1.5 nm. The parameter D represents the thickness of the defected SiO_2 layers surrounding the voids which are responsible for the PL activity.

4. Conclusions

The structure and behavior of SiO_2/Ge multilayers deposited by e-gun on Si substrate is explored after annealing at 800°C in flowing N_2 atmosphere. It is shown that such treatment drives out (outdiffuses) almost the complete Ge content, leaving behind voids in SiO_2 matrix at the former Ge layer positions. Such voids are spherical with about 3 nm diameter. The average correlation distance is about 7 nm and 4 nm in horizontal and vertical directions, respectively. It is shown that the defected SiO_2 layer around the voids causes very intensive photoluminescence with wavelengths close to 500 nm. The time-resolved PL analysis suggests that the mechanism of the observed void luminescence is similar to the one from defect layers at a Ge/SiO_2 interface. The analysis of the GISAXS data in the light of the Porod theory shows that the voids are enveloped with a shell of disordered silica about 2 nm in thickness.

With this it was shown that this approach yields a well self-organized void formation within a SiO_2 matrix at relatively low temperatures. The optical properties of such self-organized voids show interesting properties for application in silica photonics.

Conflicts of Interest

The authors declare that they have no conflicts of interest.

Acknowledgments

This work has been supported in part by the Croatian Science Foundation under Project no. 6135. The support from CREST Center, North Carolina Central University, Durham, NC, USA, is also appreciated.

References

[1] Z. Yu, A. Raman, and S. Fan, "Fundamental limit of nanophotonic light trapping in solar cells," *Proceedings of the National Acadamy of Sciences of the United States of America*, vol. 107, no. 41, pp. 17491–17496, 2010.

[2] S. Wiesendanger, M. Zilk, T. Pertsch, C. Rockstuhl, and F. Lederer, "Combining randomly textured surfaces and photonic crystals for the photon management in thin film microcrystalline silicon solar cells," *Optics Express*, vol. 21, no. 103, pp. A450–A459, 2013.

[3] Y. Tanaka, K. Ishizaki, M. De Zoysa et al., "Photonic crystal microcrystalline silicon solar cells," *Progress in Photovoltaics*, vol. 23, no. 11, pp. 1475–1483, 2015.

[4] Y. Gong and J. Vučković, "Photonic crystal cavities in silicon dioxide," *Applied Physics Letters*, vol. 96, no. 3, Article ID 031107, 2010.

[5] Y. Gong, S. Ishikawa, S.-L. Cheng, M. Gunji, Y. Nishi, and J. Vučković, "Photoluminescence from silicon dioxide photonic crystal cavities with embedded silicon nanocrystals," *Physical Review B: Condensed Matter and Materials Physics*, vol. 81, no. 23, Article ID 235317, 2010.

[6] L. Zhu, A. P. Raman, and S. Fan, "Radiative cooling of solar absorbers using a visibly transparent photonic crystal thermal blackbody," *Proceedings of the National Acadamy of Sciences of the United States of America*, vol. 112, no. 40, pp. 12282–12287, 2015.

[7] E. N. Glezer, M. Milosavljevic, L. Huang et al., "Three-dimensional optical storage inside transparent materials," *Optics Expresss*, vol. 21, no. 24, pp. 2023–2025, 1996.

[8] S. Kanehira, J. Si, J. Qiu, K. Fujita, and K. Hirao, "Periodic nanovoid structures via femtosecond laser irradiation," *Nano Letters*, vol. 5, no. 8, pp. 1591–1595, 2005.

[9] D. Barba, F. Martin, J. Demarche, G. Terwagne, and G. G. Ross, "Nanocavities and germanium nanocrystals produced by Ge ion implantation in fused silica," *Nanotechnology*, vol. 23, no. 14, Article ID 145701, 2012.

[10] C. Li, H. Feng, B. Liu et al., "Effect of nanocavities on Ge nanoclustering and out-diffusion in SiO_2," *Nanotechnology*, vol. 28, no. 3, Article ID 035707, 2017.

[11] B. Pivac, P. Dubček, J. Popović et al., "Influence of stress on the properties of Ge nanocrystals in an SiO_2 matrix," *Journal of Applied Crystallography*, vol. 49, no. 6, pp. 1957–1966, 2016.

[12] H. Amenitsch, S. Bernstorff, and P. Laggner, "High-flux beamline for small-angle x-ray scattering at ELETTRA," *Review of Scientific Instruments*, vol. 66, no. 2, pp. 1624–1626, 1995.

[13] Y. Sasaki and C. Horie, "Resonant Raman study of phonon states in gas-evaporated Ge small particles," *Physical Review B: Condensed Matter and Materials Physics*, vol. 47, no. 7, pp. 3811–3818, 1993.

[14] P. Eisenberger and W. C. Marra, "X-ray diffraction study of the Ge(001) reconstructed surface," *Physical Review Letters*, vol. 46, no. 16, pp. 1081–1084, 1981.

[15] J. R. Levine, J. B. Cohen, Y. W. Chung, and P. Georgopoulos, "Grazing-incidence small-angle X-ray scattering: new tool for studying thin film growth," *Journal of Applied Crystallography*, vol. 22, no. 6, pp. 528–532, 1989.

[16] B. Pivac, P. Dubček, I. Capan et al., "GISAXS study of Si nanostructures in SiO_2 matrix for solar cell applications," *Physica Status Solidi (a) – Applications and Materials Science*, vol. 210, no. 4, pp. 755–759, 2013.

[17] M. Störmer, J.-M. André, C. Michaelsen, R. Benbalagh, and P. Jonnard, "X-ray scattering from etched and coated multilayer gratings," *Journal of Physics D: Applied Physics*, vol. 40, no. 14, article no. 022, pp. 4253–4258, 2007.

[18] A. Coyopol, G. García-Salgado, T. Díaz-Becerril et al., "Optical and structural properties of silicon nanocrystals embedded in SiO_x matrix obtained by HWCVD," *Journal of Nanomaterials*, vol. 2012, Article ID 368268, 2012.

[19] J. Dasović, P. Dubček, I. Pucić, S. Bernstorff, N. Radić, and B. Pivac, "The interface quality of Ge nanoparticles grown in thick silica matrix," *Applied Surface Science*, vol. 414, pp. 1–7, 2017.

[20] B. Pivac, P. Dubček, J. Dasović, H. Zorc, and S. Bernstorff, "Study of the interface layers between Si nanoparticles and SiO_2 matrix deposited by e-gun evaporation," *Physica Status Solidi (b) – Basic Solid State Physics*, p. 1700633, 2018.

[21] Z. H. Li, Y. J. Gong, D. Wu et al., "A negative deviation from Porod's law in SAXS of organo-MSU-X," *Microporous and Mesoporous Materials*, vol. 46, no. 1, pp. 75–80, 2001.